Evolution of Texture and Microstructure in a Thermomechanically Processed Al-Li-Cu-Mg Alloy

A.K. SINGH, G.G. SAHA, A.A. GOKHALE, and R.K. RAY

The development of texture and microstructure in a thermomechanically processed quaternary Al-Li-Cu-Mg alloy has been investigated. Textures on both the surface (1/8 thickness (T)) and midthickness levels of specimens were measured using the conventional pole figure as well as the orientation distribution function (ODF) method. Microstructural characterization was carried out with the help of optical microscopy and transmission electron microscopy (TEM). The processing schedule involved hot cross rolling, followed by several stages of cold rolling (CR) with intermediate solution treatments (STs). A marked through-thickness texture inhomogeneity developed in the processed sheets during the course of thermo mechanical treatment (TMT). In general, the texture produced at the midthickness level was 2 to 3 times sharper than the texture at the surface.

The alloy, after hot cross rolling, showed nearly equally strong Bs $\{110\}\langle 112\rangle$ and Bs/S $\{168\}\langle 211\rangle$ components at midthickness. After three cycles of cold rolling (CR) and solution treatments (STs), the overall texture intensity came down by a factor of nearly 2. The final processed sheet material showed a moderately strong Bs and a predominant S $\{123\}\langle 634\rangle$ component at midthickness. Solution treatments did not produce much change in the texture of the cold-rolled materials. Microstructural evidence indicated extensive recovery and, at best, partial recrystallization of the deformed structure. No significant effect of second-phase particles in texture development was noticed.

I. INTRODUCTION

THE Al-Li alloys, because of their low density and high modulus, are becoming attractive for applications in the aerospace industries.[1,2,3] A desired characteristic of these materials for such applications is uniformity of mechanical properties in all directions. In practice, however, these materials are prone to develop marked anisotropy of mechanical properties after processing.[4] This has been attributed to either the preferred orientation of grains, *i.e.*, texture,[5] or to morphological features such as precipitates (notably δ),[6] elongated grain boundaries, and incomplete recrystallization.[7] Among these, texture appears to play the dominant role in yield strength anisotropy,[5] while the remaining factors influence anisotropy of toughness and fatigue properties.[7]

The evolution of texture in Al-Li alloys has been studied by several workers.[8,9,10] Vasudevan *et al.*[8] investigated the effect of composition on the development of texture in hot-rolled binary Al-Li alloys. They observed primary Goss and secondary Cube components at low Li levels and well-developed β fibre in alloys with high Li content. Engler *et al.*[9] have studied the specific roles of Li, Zr, and Cu in Al-Li base alloys in influencing texture evolution during hot rolling. It was reported that hot rolling of Zr containing alloys led to a strong Bs texture component, while CR of all the alloys resulted in the usual Talyor type β fibre components. Texture evolution in a 8090 Al-Li alloy was extensively studied by Bull and Lloyd[10] as a function of hot rolling and CR, hot cross rolling, and postrolling solution treatments.

The aforementioned studies on texture evolution in Al-Li alloys were not supported by detailed microstructural observations. The textural information, in most cases, was presented in the form of pole figures and was therefore only qualitative in nature. In the present work, the evolution of texture in a quaternary Al-Li-Cu-Mg alloy (similar to 8090) has been studied, in conjunction with extensive microstructural characterization, in hot-rolled, cold-rolled, and heat-treated conditions. The textures were measured using both the pole figure and the orientation distribution function (ODF) methods. The processing here consisted of hot cross rolling followed by straight CR, ST (and further CR, *etc.*), which was quite different from the schedule used by Bull and Lloyd.[10] The aim of the present work was to evaluate the effect of the processing schedule on microstructural and textural development with special reference to the possible reduction of the texture severity in this alloy. Finally, the results obtained in the present work were compared with those of Bull and Lloyd[10] and others.

II. EXPERIMENTAL

A. *Material Processing*

The chemical analysis of the alloy is given in Table I. The alloy was chill cast in a mild steel mold in the form of a slab. The details of melting and casting are reported elsewhere.[11] The cast slab was homogenized at 540 °C for 40 hours followed by forced air cooling. The homogenized slab was machined to 300 × 300 × 35-mm size. It was then straight hot rolled by 41 pct reduction along the direction of casting and then cross rolled by another 41 pct

A.K. SINGH, G.G. SAHA, and A.A. GOKHALE, Scientists, are with the Defence Metallurgical Research Laboratory, Hyderabad—500058, India. R.K. RAY, Professor, is with the Department of Materials and Metallurgical Engineering, Indian Institute of Technology, Kanpur—208016, India.

Manuscript submitted May 9, 1997.

Table I. Composition of Al-Li-Cu-Mg Alloy Used in This Study

Element	Wt Pct
Li	1.96
Cu	1.14
Mg	0.86
Zr	0.10
Be	0.013
Fe	0.062
Si	0.056
Al	balance

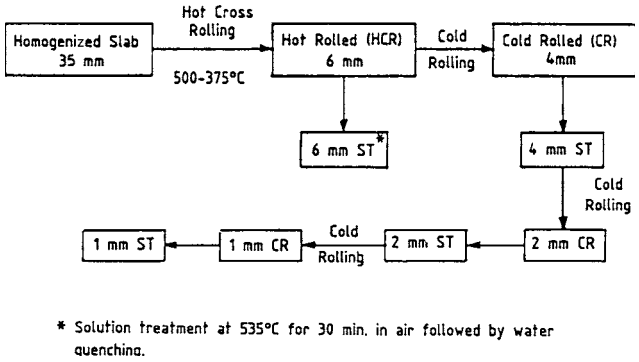

Fig. 1—Processing schedule of the Al-Li-Cu-Mg alloy.

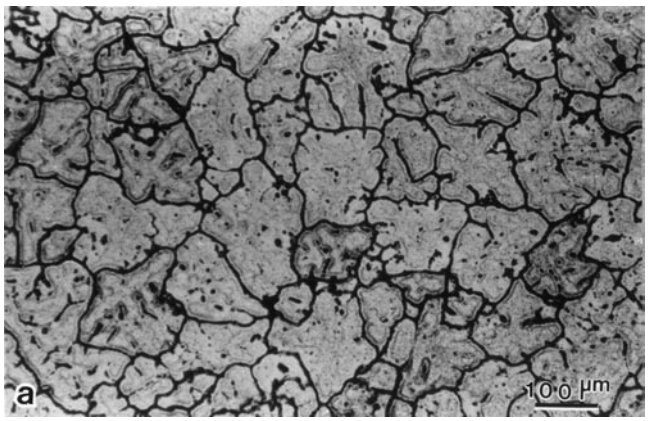

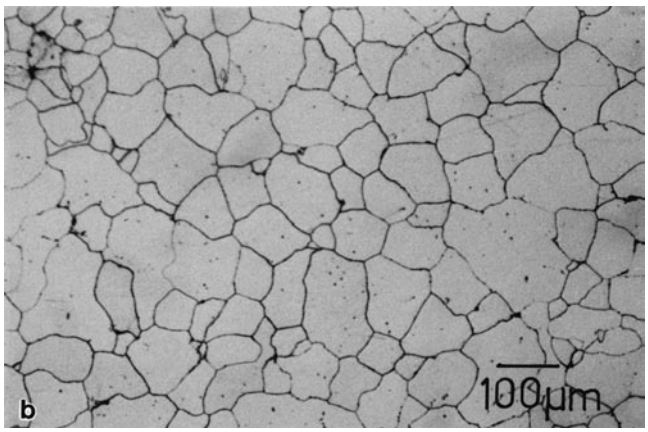

Fig. 2—Optical micrographs of the alloy in (*a*) as-cast condition and (*b*) after homogenization.

in a direction normal to the former, within a temperature range of 500 °C to 375 °C. The hot-cross-rolled (HCR) sheet of ~6-mm thickness was further cold rolled to 4-mm thickness and then solution treated. The solution-treated material was further cold rolled to 2-mm thickness followed by another solution treatment. The 2-mm thickness sheet was finally cold rolled to 1-mm thickness and then solution treated again. All STs were carried out in an air furnace at 535 °C for 30 minutes followed by water quenching. The processing schedule is shown in the form of a block diagram in Figure 1.

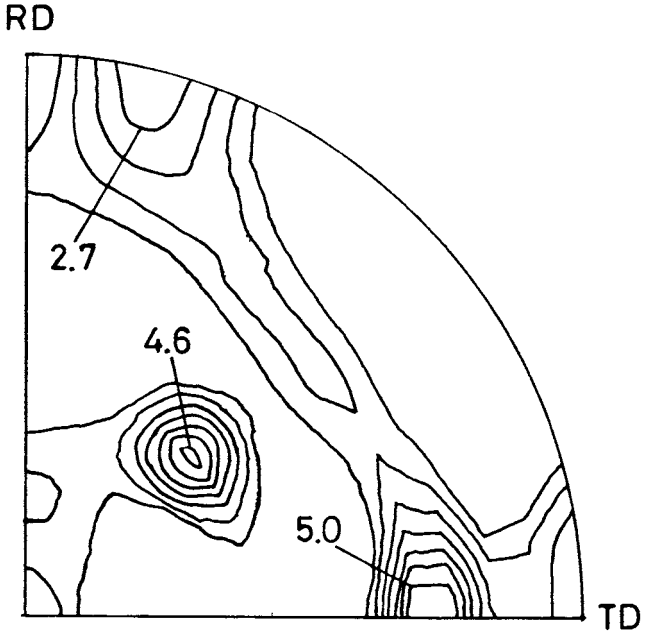

Fig. 3—{111} pole figure showing HCR texture of the 6-mm HCR specimen (1/2 T level).

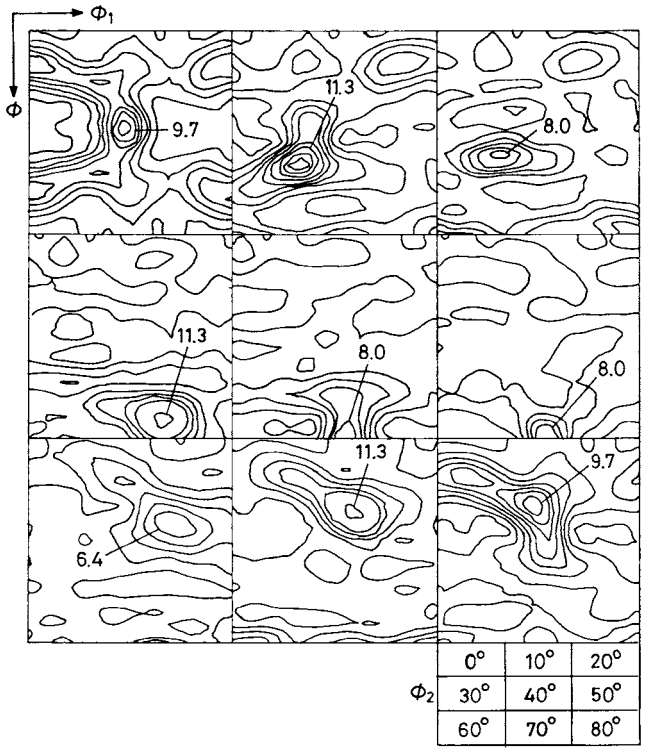

Fig. 4—Constant ϕ_2 sections of the ODF for the 6-mm HCR specimen (1/2 T level).

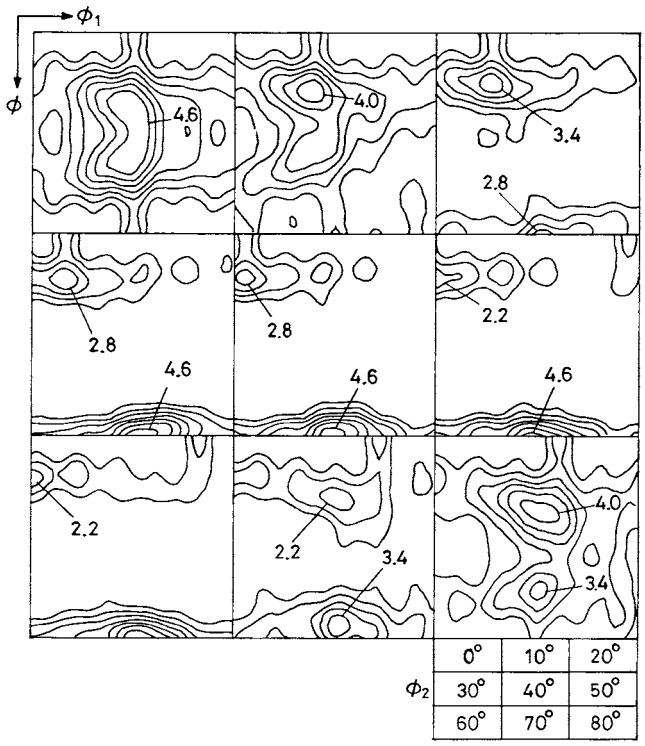

Fig. 5—Constant ϕ_2 sections of the ODF for the 6-mm HCR specimen (1/8 T level).

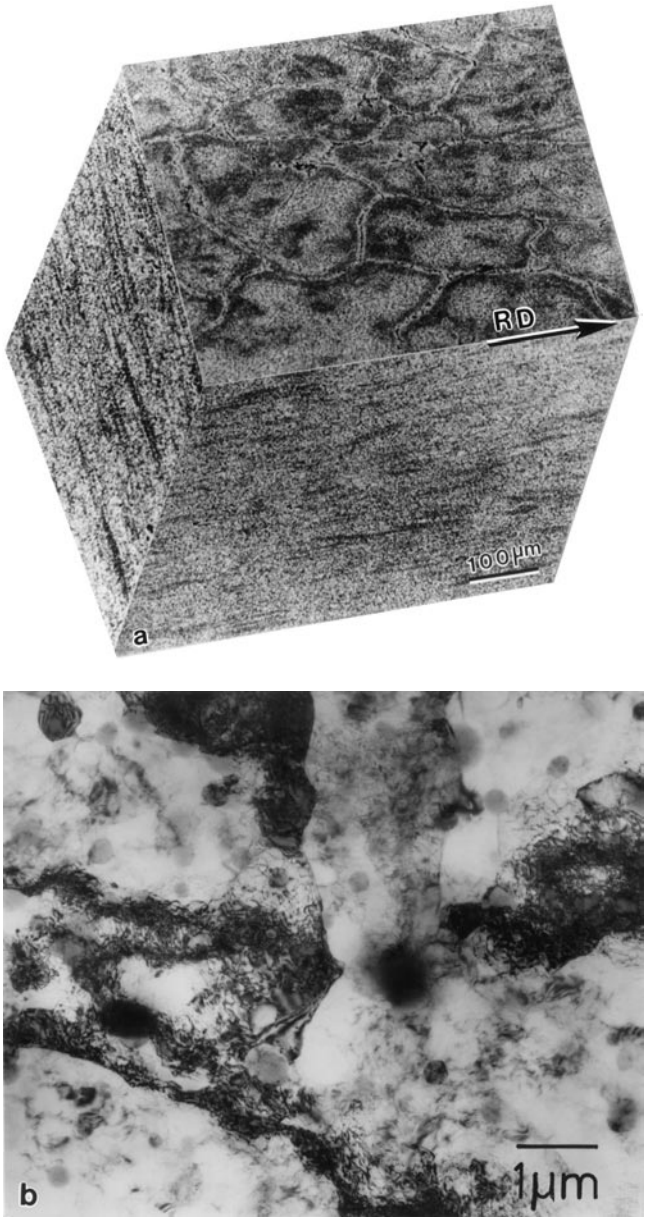

Fig. 6—(*a*) 3-D optical micrograph of the alloy in the 6-mm HCR condition. (*b*) Bright-field TEM micrograph of the 6-mm HCR specimen.

Texture analysis, optical metallography, and transmission electron microscopy (TEM) were carried out for the HCR, CR, and ST conditions at different stages of reduction from 6 to 1 mm thickness.

B. *Texture Measurement*

Texture measurements were carried out on sheet specimens of 25 × 16-mm size. Since Al-Li alloys are known to develop a strong texture gradient[12] along the sheet thickness during processing, all texture measurements were carried out at similar thickness levels (1/2 and 1/8 thicknesses (T's) from the surface) in all the samples. A SIEMENS* D-500 texture goniometer using Mo K_α radiation was employed for data collection for the construction of {111}, {200}, {220}, and {311} pole figures, after the Schulz backreflection technique.[13] These pole figures were corrected for defocusing and absorption using a powder sample of commercially pure Al. Orientation distribution function plots were calculated from the pole figure data, following the formulation of Bunge.[14] The ODFs were presented as plots of constant ϕ_2 sections with isointensity contours in the Euler space defined by the Euler angles ϕ_1, ϕ, and ϕ_2.

*SIEMENS is a trademark of Siemens Electrical Equipment, Toronto.

C. *Optical and Electron Microscopy*

The microstructures of HCR, CR, and ST specimens were observed using both optical microscopy and TEM. In each sample, optical metallography was carried out for all three planes with plane normals along the normal direction (ND), the rolling direction (RD), and the transverse direction (TD). The specimens were polished per standard practice used for aluminum alloys and etched using Kellar's reagent (95 pct water, 2.5 pct nitric acid, 1.5 pct hydrochloric acid, and 1 pct hydrofluoric acid). Thin foils of rolled sheet samples for TEM work were prepared by twin jet electropolishing technique using an electrolyte of 33 pct nitric acid and 67 pct methanol (by volume) at a temperature of 243 K. The thin foils so prepared were examined under a PHILIPS* EM430 transmission electron microscope operated at 300 kV.

*PHILIPS is a trademark of Philips Electronic Instruments Corp., Mahwah, NJ.

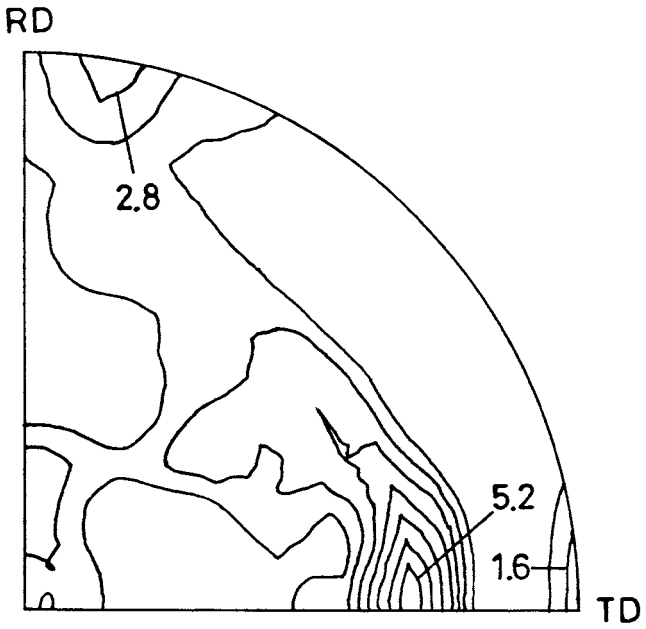

Fig. 7—{111} pole figure showing the texture of the 6-mm ST specimen (1/2 T level).

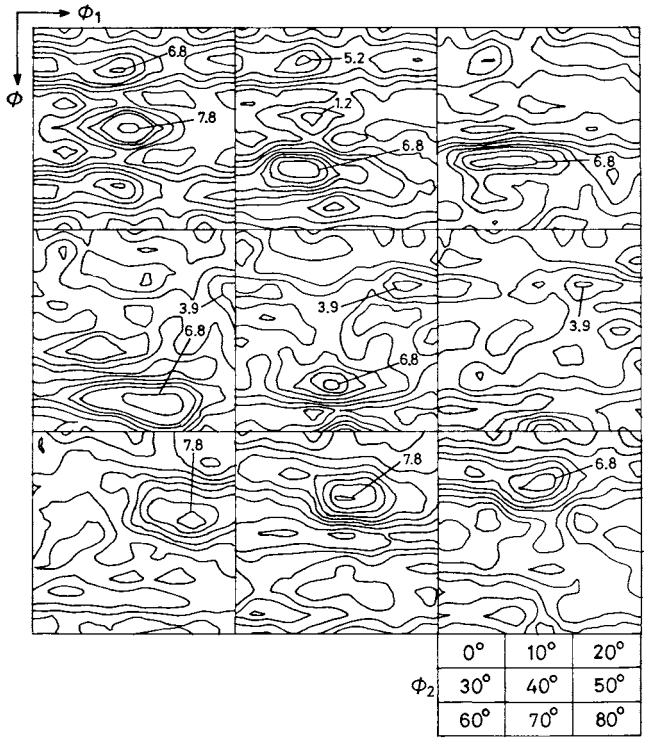

Fig. 8—Constant ϕ_2 sections of ODF for the 6-mm ST specimen (1/2 T level).

III. RESULTS AND DISCUSSION

A. *As-Cast and Homogenized Material*

The as-cast structure reveals equiaxed dendritic microstructure with average grain size in the range of 125 to 150 μm (Figure 2(a)). Typical as-cast microstructural features of aluminum alloys, such as inclusions, segregation, and nonequilibrium solidification product phases, are present in this alloy also. Homogenization (Figure 2(b)) leads to the disappearance of the segregation pattern and almost complete dissolution of the nonequilibrium solidification product phases. The texture of the homogenized material was found to be nearly random.

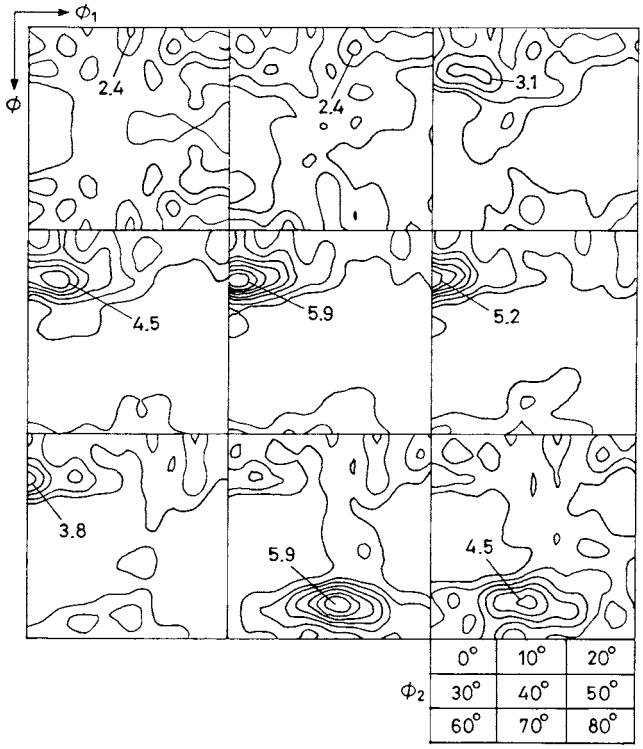

Fig. 9—Constant ϕ_2 sections of ODF for the 6-mm ST specimen (1/8 T level).

B. *Textures and Microstructures after Hot Cross Rolling and ST*

The (111) pole figure (Figure 3) of the 6-mm HCR specimen at the 1/2 T level shows a moderately strong texture. The important texture components determined from the corresponding ODF (Figure 4) are the Bs {110} ⟨112⟩ ($f(g)$ = 9.5) and a tube of S {123} ⟨634⟩, showing a maximum $f(g)$ = 11.4 at the location midway between the S and the Bs/S {168} ⟨211⟩. The ODF plot taken from the 1/8 T level (Figure 5) indicates that the texture intensity at this thickness level is much less (<50 pct) than that at the midthickness (1/2 T) region. The texture components here are {110} ⟨112⟩ ($f(g)$ = 4.6), {168} ⟨211⟩ ($f(g)$ = 4.0), and {169} ⟨321⟩ ($f(g)$ = 4.0).

Figure 6(a) shows the three-dimensional (3-D) optical micrograph of the alloy in the HCR condition. The microstructure consists of pancake-shaped grains with grain boundaries decorated by second-phase particles. The TEM study of this specimen (Figure 6b) shows the presence of icosahedral T_2 (AL_6CuLi_3) phase and also particles of the type Al-Cu-Fe and Al-Cu-Ti.[15] There is no evidence of recrystallization at this stage. It may be mentioned here that the T_2 phase was not observed in any condition beyond the HCR stage.

The ST after hot cross rolling reduces the texture intensity at the 1/2 T level substantially, as can be seen in the relevant (111) pole figure (Figure 7). The corresponding ODF (Figure 8) again shows a moderately strong Bs and a

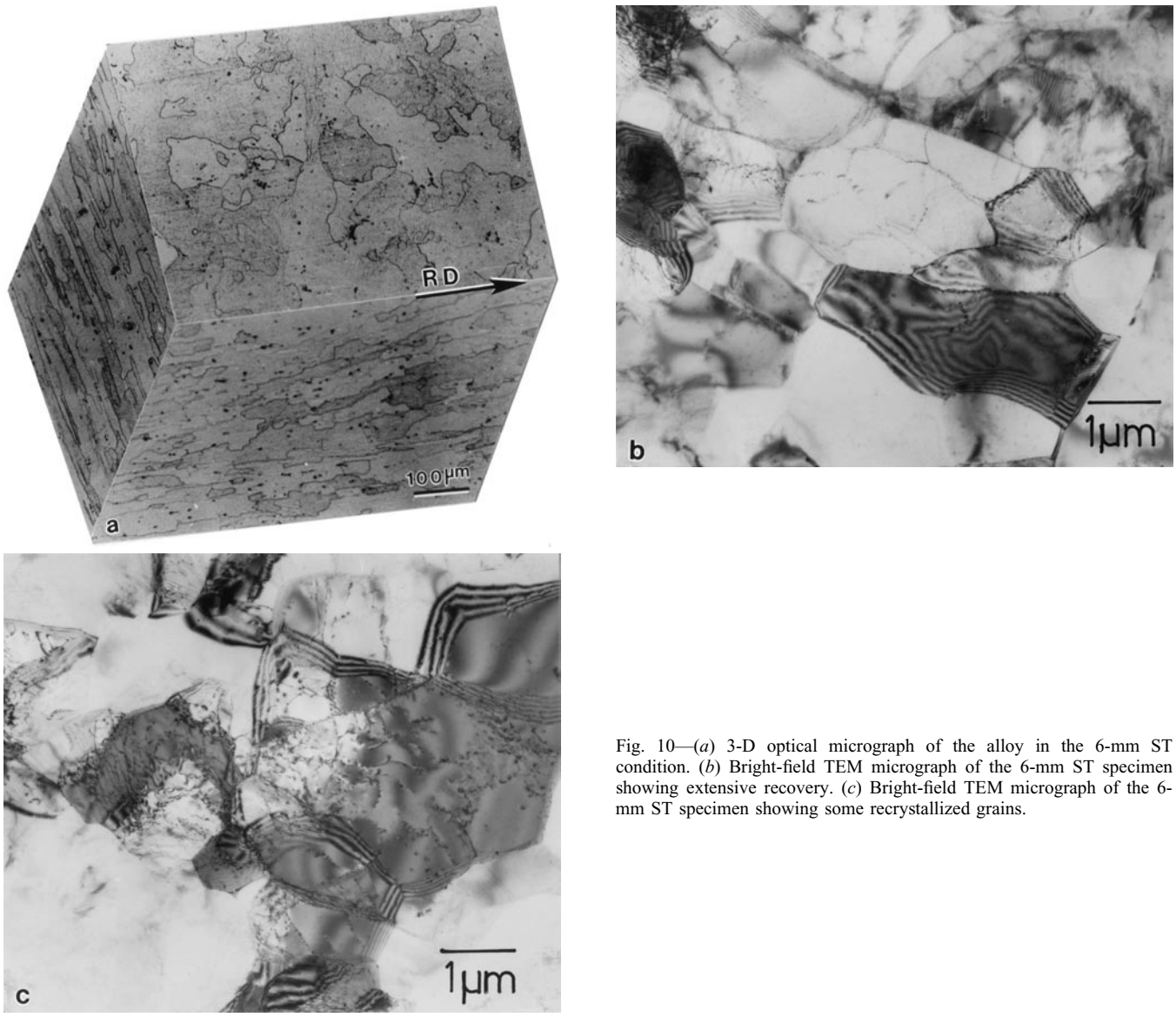

Fig. 10—(*a*) 3-D optical micrograph of the alloy in the 6-mm ST condition. (*b*) Bright-field TEM micrograph of the 6-mm ST specimen showing extensive recovery. (*c*) Bright-field TEM micrograph of the 6-mm ST specimen showing some recrystallized grains.

S tube of nearly uniform intensity ($f(g) = 7.8$). In addition, a reasonably strong $\{013\}\ \langle 331\rangle$ component is also observed, having $f(g)$ of 6.5. The ODF of the solution-treated specimen at the 1/8 T level (Figure 9), however, shows one major component only, located at $\{113\}\ \langle 110\rangle$, with $f(g)$ of nearly 6.0.

Figure 10(a) shows the microstructure of the HCR alloy after ST (6-mm ST). It is quite obvious that the alloy appears to have undergone partial recrystallization at this stage. It is also seen that, in spite of recrystallization, the lamellar geometry of the grains is observed to persist in the transverse and longitudinal sections. The TEM study of this specimen shows the presence of clear subgrain structure (Figure 10(b)) at most places, indicating extensive recovery. Presence of some well-defined recrystallized grains can also be seen (Figure 10(c)) at a few places.

C. *Textures and Microstructures after CR and ST*

The series of six (111) pole figures (Figure 11) depict the changes in texture that occur at the 1/2 T level during the successive CR/ST cycles to which the 6-mm HCR samples were subjected during processing. The texture is found to intensify as the 6-mm HCR sample is cold rolled to 4-mm thickness, without any significant changes in the nature of the components (Figure 11(a)). The subsequent ST leads to a decrement in the intensity of the texture, followed by a sharpening again as the material is cold rolled to 2-mm thickness. This cycle of sharpening of texture with CR and its weakening after subsequent ST persists until the final stage of processing (Figures 11(b) and (f)).

The texture of the specimen cold rolled to 1-mm thickness, followed by ST, is decidedly the weakest, and is almost half as strong as the texture of the first cold-rolled material (4-mm thickness). However, the very fact that the material possesses a reasonably strong texture, even at the final stage of processing, indicates the persistence of crystallographic texture in this alloy during processing.

The preceding observations are further corroborated from the study of the relevant ODF plots. Figure 12 shows a composite plot of the $\phi_2 = 0$, 30, 40, and 60 deg sections of the ODFs (at the 1/2 T level) of the preceding six ma-

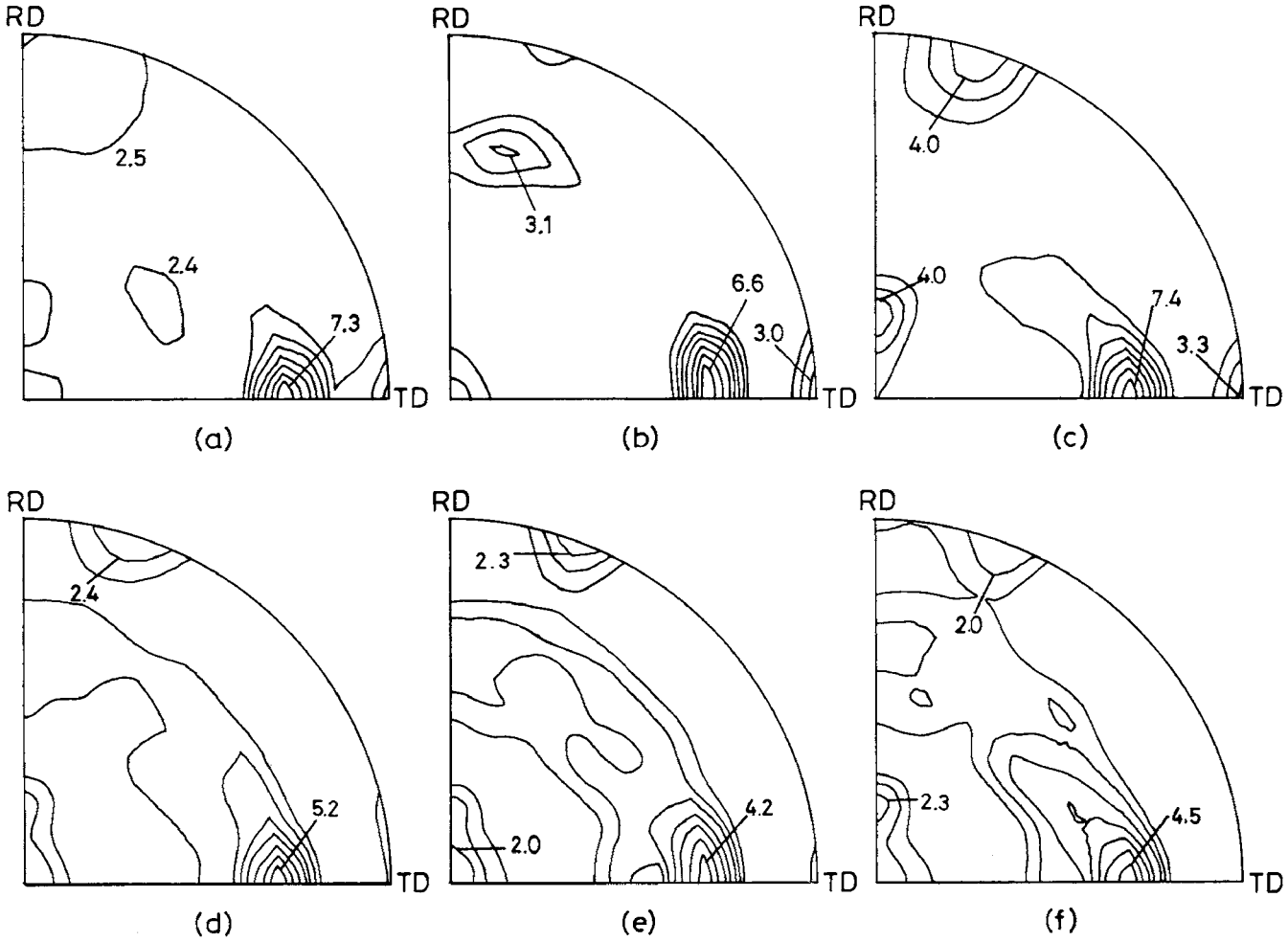

Fig. 11—{111} pole figures (at 1/2 T level) of (*a*) 4-mm CR, (*b*) 4-mm ST, (*c*) 2-mm CR, (*d*) 2-mm ST, (*e*) 1-mm CR, and (*f*) 1-mm ST.

terials. The information contained in this plot can be described as follows. The strongest texture component in the 4-mm CR specimen is a tube of orientations around the S and the {013} ⟨331⟩ ($f(g)$ = 9.2). In addition, there is a weak Bs component also with $f(g)$ = 3.2. Subsequent ST leads to a sharpening of the Bs component to $f(g)$ = 8.1, while the $f(g)$ value for the S component decreases from the previous 11.0 to around 7.0. There is practically no change in the intensity of the {013} ⟨331⟩ component. Cold rolling to 2-mm thickness introduces a weak Cu {112} ⟨111⟩ component ($f(g)$ = 4.5), whereas the S component sharpens significantly to $f(g)$ of about 12.2 and the Bs component also strengthens marginally; the intensity of the {013} ⟨331⟩ component drops to $f(g)$ = 6.7. The overall sharpnesses of all the preceding components decrease with subsequent ST. While CR to 1-mm thickness improves the intensity of the Cu component and decreases the intensities of the other components somewhat, the final ST appears to cause a general small decrement in the intensities of all the components.

A composite plot of the ϕ_2 = 0, 30, 40, and 60 deg sections of ODFs (at 1/8 T level) from the cold-rolled as well as the cold-rolled and solution-treated samples is depicted in Figure 13. The salient features of the texture variations at this level of thickness, as a function of processing, can be described as follows. Cold rolling of the 6-mm ST sample produces a reasonably strong {001} ⟨110⟩ ($f(g)$ = 5.0) plus a few other weak components obtained by rotation of the preceding component around the ND. Subsequent ST appears to intensify the {001} ⟨110⟩ component marginally ($f(g)$ = 5.2). Cold rolling to a thickness of 2 mm produces essentially a pure metal or copper type texture, characterized by a strong S ($f(g)$ = 8.0) and moderate Cu ($f(g)$ = 4.5) and Bs ($f(g)$ = 3.0) components. Solution treatment of this material brings down the intensities of the preceding components and also produces a host of weak orientations of the {001} ⟨*uvw*⟩ type. When this material is cold rolled to 1-mm thickness, the texture components do not change, but the overall texture sharpens marginally. Subsequent ST does not change the general character of the CR texture, but causes perceptible randomization.

Figures 14(a) and (b) show the microstructure of the alloy in 4-mm CR and 4-mm ST conditions, respectively. The 4-mm CR microstructure (Figure 14(a)) appears similar to that of 6-mm HCR; however, 4-mm ST (Figure 14(b)) shows a larger extent of recrystallization than 6-mm ST. The TEM microstructures (Figures 15(a) and (b)) of the 4-mm ST specimen show the presence of fine subgrains as well as completely recrystallized grains. The greater degree of recrystallization in the 4-mm ST condition as compared

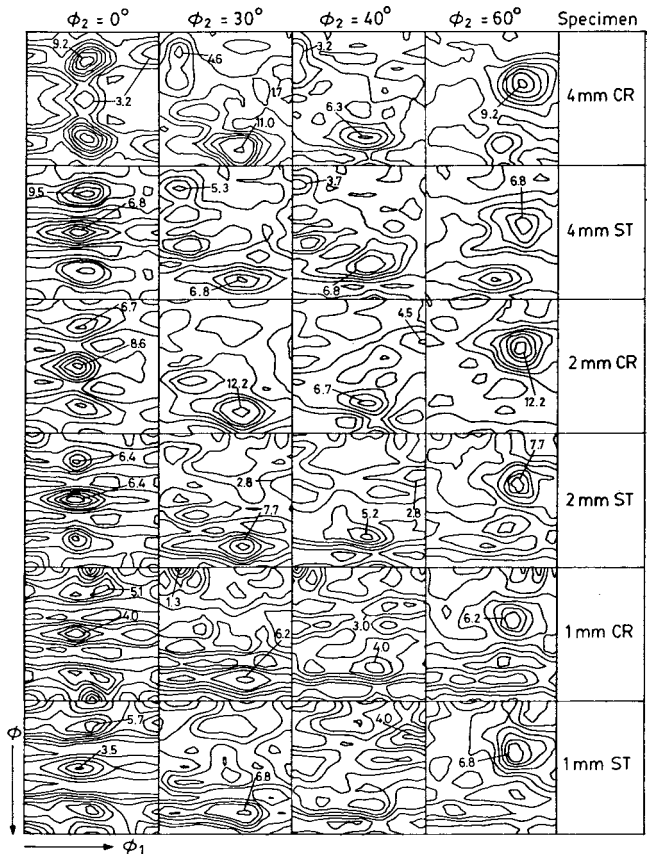

Fig. 12—Composite plot of the ϕ_2 = 0, 30, 40, and 60 deg sections of the ODFs of the six materials (at 1/2 T level) mentioned in Fig. 11.

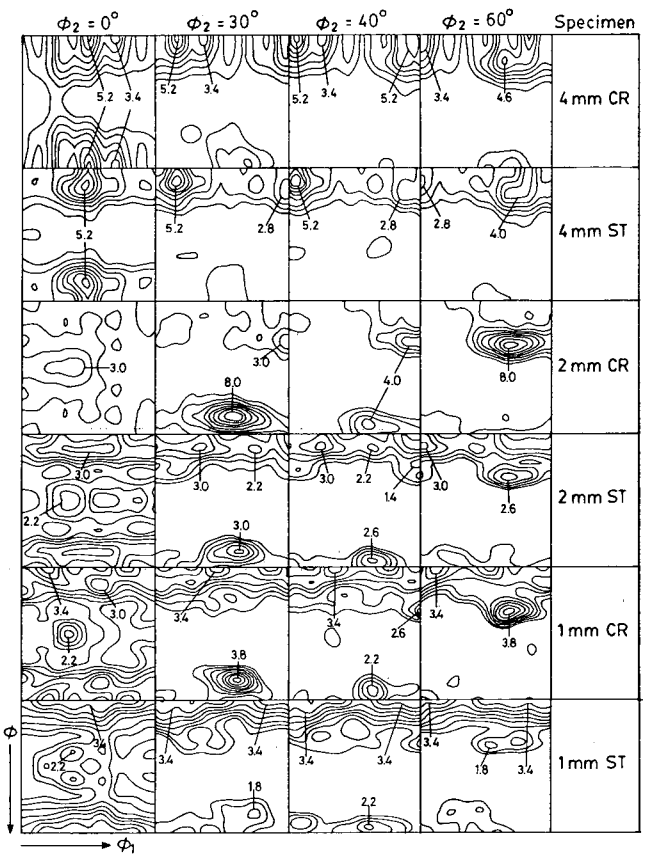

Fig. 13—Composite plot of the ϕ_2 = 0, 30, 40, and 60 deg sections of the ODFs of the six materials (at 1/8 T level) mentioned in Fig. 11.

to the 6-mm ST is obviously due to the larger stored strain energy, providing a large driving force for recrystallization in the case of the cold-rolled specimens.

Figures 16(a) and (b) show the 3-D optical microstructures of the alloy in 2-mm CR and 2-mm ST conditions, respectively. The microstructure in Figure 16(a) (2-mm CR) is entirely different from the microstructures of 6-mm HCR and 4-mm CR conditions. The 2-mm CR microstructure shows well-defined grain boundaries and the relative absence of intra- and intergranular precipitates seen in 6-mm HCR and 4-mm CR conditions. These microstructural differences can be attributed to the partial recrystallization and precipitate dissolution accompanying the ST of the 4-mm CR samples carried out prior to CR to 2-mm thickness. The microstructure of the alloy in 2-mm ST condition (Figure 16(b)) shows a higher degree of recrystallization in the sample, although the grains appear pancake shaped.

Figures 17(a) and (b) show the 3-D optical microstructures of the alloy in 1-mm CR and 1-mm ST conditions. The microstructure of the 1-mm CR specimen shows elongated grains as in the case of the 2-mm CR specimen, although the grains are somewhat coarser in the 1-mm CR condition (Figure 17(a)). The solutionized specimen (1-mm ST) shows a partially recrystallized microstructure (Figure 17(b)). The TEM micrograph of the 1-mm CR specimen (Figure 18(a)), however, shows a highly recovered substructure and clear-cut subgrains. The subsequent ST leads to partial recrystallization in many parts of the sample (Figure 18(b)).

D. *Texture Development and the Through-Thickness Texture Inhomogeneity during Processing*

The CR texture of pure Al, which has a rather high stacking fault energy, is essentially pure metal type, consisting of the Cu, Bs, and S components, with the last component being the strongest.[16] Microstructural evidence has shown that no significant recrystallization occurs in the present alloy either during hot rolling or after CR and/or subsequent STs. The absence of the cube $\{100\}\ \langle 001\rangle$ component in the annealed textures also corroborates this. Zirconium is known to effectively inhibit static or dynamic recrystallization.[9,10] The high level of Li also makes the recrystallization process rather sluggish.[10] The presence of significant amounts of Zr and Li in the present alloy must have prevented extensive recrystallization during processing. Thus, the texture developed is not expected to be much different from those produced in similar alloys by CR.

Bull and Lloyd[10] studied the evolution of texture in a 8090 Al-Li alloy as a function of hot rolling and CR. They found typical Cu type texture due to straight hot rolling and CR. To study the effect of hot cross rolling, the material was initially straight hot rolled 90 pct parallel to the casting direction and then cross rolled in a perpendicular direction by different amounts. They observed that the initial Cu type rolling texture spreads in a CR direction and then further evolves into the Bs $\{110\}\ \langle 112\rangle$ texture after 50 pct reduction. The pole figure of their material at this stage qualitatively resembles the pole figure obtained for the present

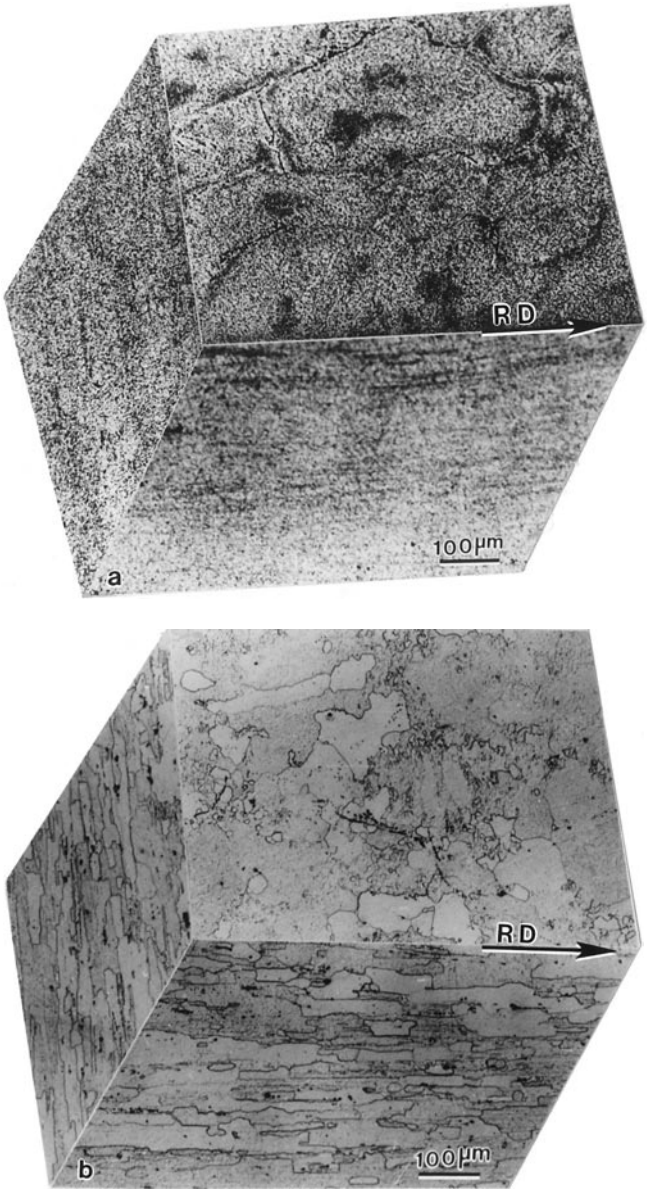

Fig. 14—3-D optical micrograph of the alloy in the (*a*) 4-mm CR and (*b*) 4-mm ST conditions.

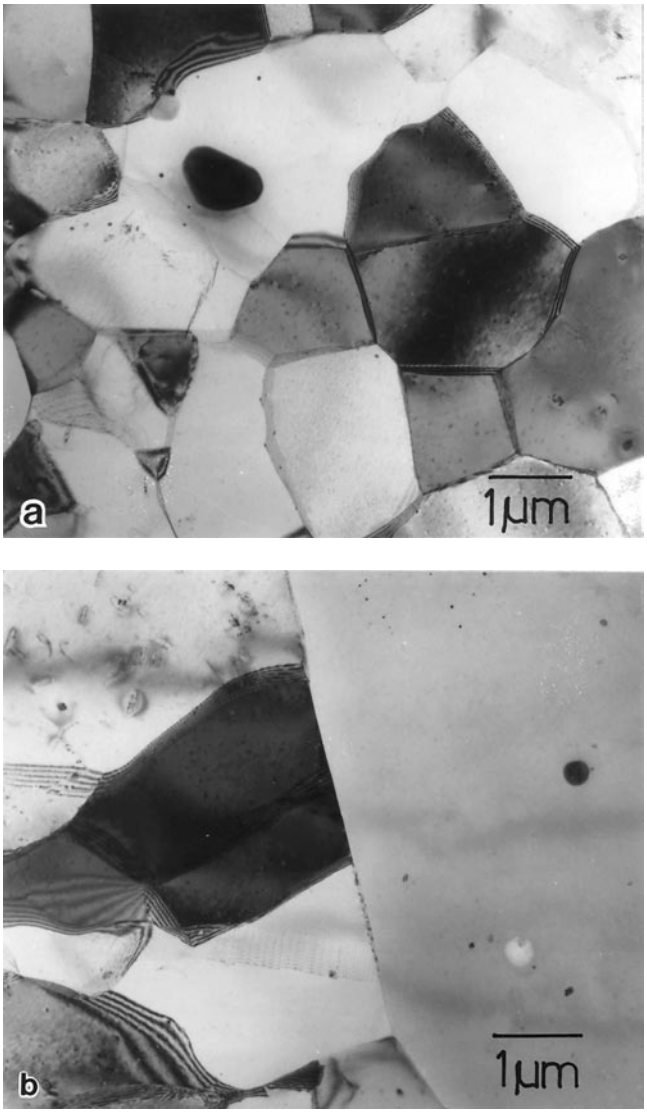

Fig. 15—Bright-field TEM micrographs of the 4-mm ST specimen showing (*a*) the presence of fine subgrains and (*b*) completely recrystallized grains.

alloy in the 6-mm HCR condition. Detailed ODF measurement at this condition on the present alloy, however, clearly indicates that in addition to the {110} ⟨112⟩ component, there is an equally strong component near the Bs/S location (Figure 4).

In the absence of any ODF data in Bull and Lloyd's[10] article, it is difficult to make a proper comparison between the present results and theirs. One obvious reason for the apparent discrepancy could be due to the fact that whereas Bull and Lloyd HCR their material after subjecting it to straight hot rolling by an amount as high as 90 pct, in the present alloy, HCR was performed after it was straight hot rolled by a moderate amount of 41 pct only. Thus, the overall texture intensity in the present alloy was presumably much weaker than in the material used by Bull and Lloyd, prior to the hot-cross-rolling operation.

Three cycles of CR/ST have been used during processing in the present investigation. Although, qualitatively, the texture components (at 1/2 T level) in the initial 4-mm CR and the final 1-mm ST samples are not much different, the overall texture intensity comes down by nearly a factor of 2 at the end of the entire process. This clearly points to a limited amount of randomization, which has been achieved by using the three cycles of CR/ST. These results also demonstrate the difficulties involved in deriving this material in a weakly textured condition. Although the texture at the 1/8 T level is somewhat different and weak as compared to that at the 1/2 T level, the texture here also persists with cycles of CR/ST, as practiced in this investigation. The {001} ⟨110⟩ component, which has been associated with the texture at this thickness level, must owe its origin to the high level of shearing at and near the surface, and this and related components are found to be present in the texture even after the final processing stage.

The β-fibre plots (Figures 19(a) and (b)) for the alloy, at various stages of processing and for both the thickness levels 1/2 and 1/8 T, help to illustrate the successive stages of texture development in the experimental alloy during pro-

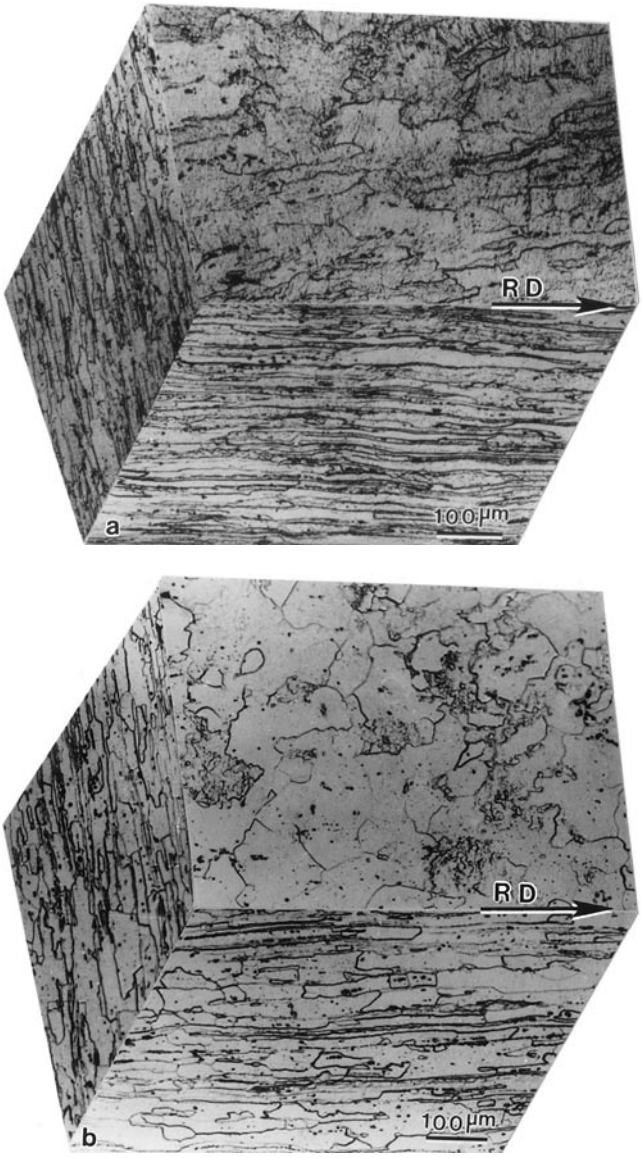

Fig. 16—3-D optical micrographs of the alloy in the (*a*) 2-mm CR and (*b*) 2-mm ST conditions.

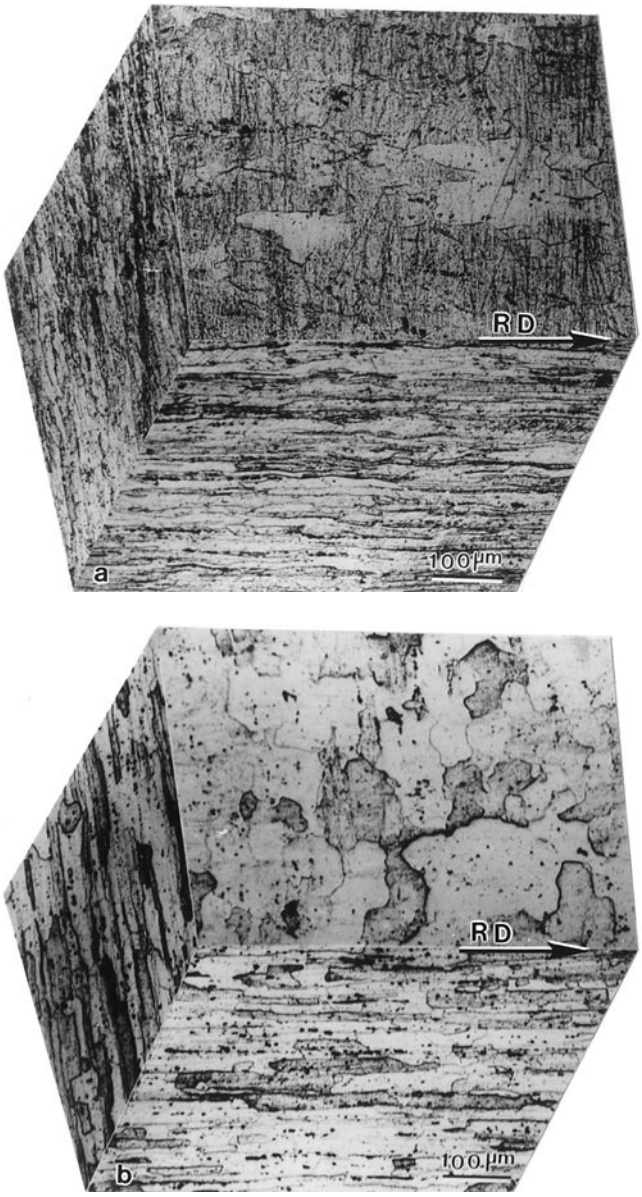

Fig. 17—3-D optical micrographs of the alloy in the (*a*) 1-mm CR and (*b*) 1-mm ST conditions.

cessing. At the same time, these diagrams help to illustrate the substantial texture inhomogeneity produced in this material in the through-thickness direction.

In the literature, it has often been mentioned that processed Al-Li base alloys are more textured than the conventional high strength aluminum alloys, and as a result, these alloys exhibit strong yield strength anisotropy within the sheet and in the through-thickness direction.[4–7] It has often been shown that this anisotropy is due to the formation of a strong texture consisting predominantly of the Bs $\{110\}\ \langle 112\rangle$ orientation.[9] The results of the present investigation have clearly indicated that the high intensity of the Bs component can be brought down to nearly half its value by repeated CR/ST treatments (Figure 19(a)). Nevertheless, the presence of a rather strong texture at the 1/2 T level, consisting predominantly of the S $\{123\}\ \langle 634\rangle$ component and a marked through-thickness texture gradient, will continue to be a matter of concern when any serious engineering application of this alloy is contemplated.

The yield stress anisotropy of Al-Li alloys has often been attributed to both crystallographic texture and precipitates.[17] In this context, it would be interesting to see if and how texture development in this alloy could have been affected by the presence of precipitate particles, although no conscious effort was made in this work to evaluate this aspect. As mentioned earlier, the TEM microstructure of the 6-mm HCR specimen showed the presence of particles of the T_2 phase (Figure 6(b)); these were, however, not observed beyond the HCR stage. Again, the high density of second-phase particles present in the optical microstructure of the 4-mm CR specimen (Figure 14(a)) appeared to go into solution during the subsequent ST. These particles as well as the ones seen in the optical micrographs of the 1-mm CR and 1-mm ST specimens (Figures 17(a) and (b)) were too coarse to interfere effectively with dislocation movement during hot rolling and/or subsequent STs. On the other hand, the TEM microstructures in the CR/ST con-

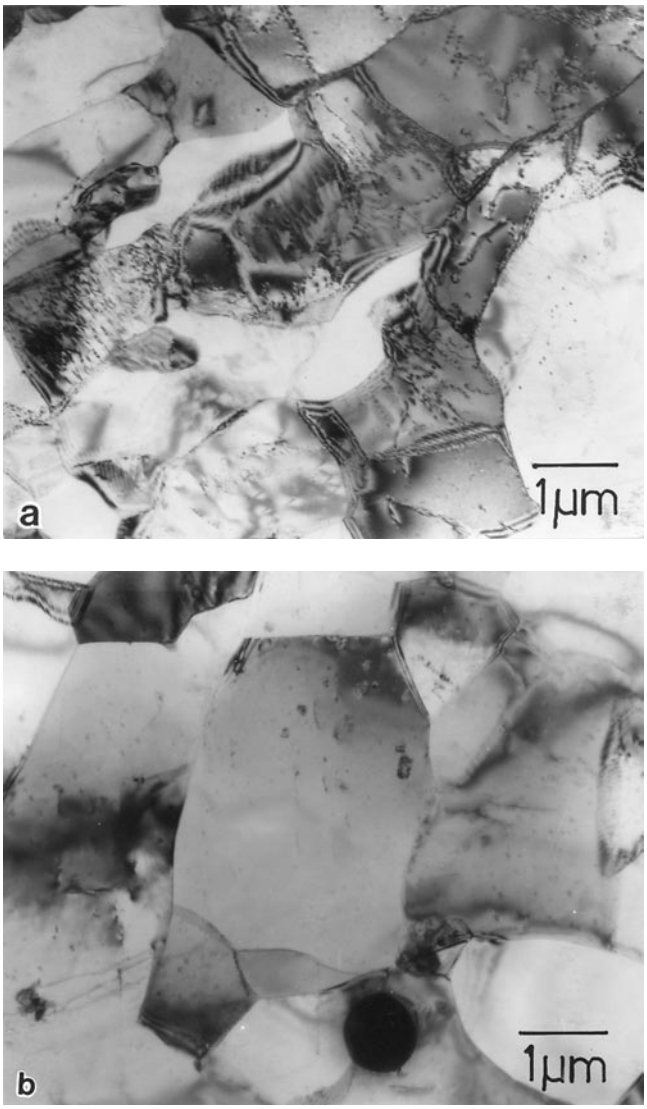

Fig. 18—(*a*) Bright-field TEM micrograph of the 1-mm CR specimen showing recovered substructure. (*b*) Bright-field TEM micrograph of the 1-mm ST specimen showing partial recrystallization.

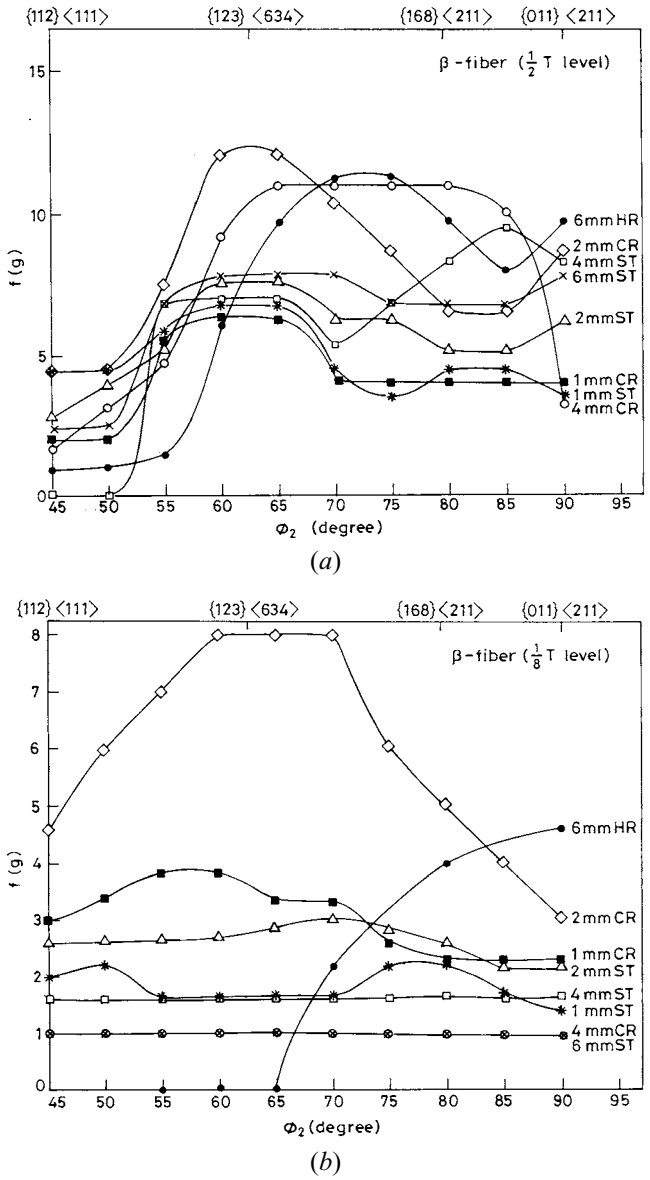

Fig. 19—β-fibre plots for the alloy at various stages of processing (*a*) at the 1/2 T level (*b*) at the 1/8 T level.

ditions showed invariably a rather clean matrix without much of a fine precipitation in almost all the samples. Solution treatment after CR produced mostly extensive recovery and only partial recrystallization at a few places, and then also no evidence of any particle stimulated nucleation of grains or subgrains could be obtained. The previous observations, therefore, rule out any significant effect of the second-phase particles in texture development in the present alloy.

IV. CONCLUSIONS

1. Thermomechanical processing of Al-Li-Cu-Mg quaternary alloy produces a marked through-thickness texture inhomogeneity.
2. At any particular stage of processing, the texture at the midthickness region is 2 to 3 times sharper than that at the surface.
3. Hot cross rolling texture at the midthickness level consists of two nearly equally strong components, Bs $\{110\}\langle 112\rangle$ and Bs/S $\{168\}\langle 211\rangle$.
4. Three cycles of CR followed by ST bring down the overall texture intensity by a factor of around 2.
5. The texture of the finally processed 1-mm-thick sheets consisted of a moderately strong Bs and a strong S $\{123\}\langle 634\rangle$ component.
6. Solution treatment of the cold-rolled material produces extensive recovery and only partial recrystallization.
7. Second-phase particles do not seem to affect texture development in this alloy during processing.

ACKNOWLEDGMENTS

The authors are indebted to Dr. D. Banerjee, Director, Defence Metallurgical Research Laboratory (Hyderabad), for encouragement and support and are also grateful to him for his permission to publish this article. The financial support of the Aeronautical Research and Development Board

(AR&DB), DRDO, Ministry of Defence, Government of India, is also gratefully acknowledged.

REFERENCES

1. *Aluminium-Lithium Alloys III*, C. Baker, P.J. Gregson, S.J. Harries, and C.J. Peel, eds., The Institute of Metals, London, 1986.
2. *4th Int. Conf. on Aluminium-Lithium Alloys*, G. Champier, B. Dubost, D. Mianny, and L. Sabetay, eds.; appeared in *J. Phys.*, 1987, Coll. C3, vol. 48 (9).
3. *Aluminium-Lithium Alloys V*, T.H. Sanders, Jr. and E.A. Starke, Jr., MCEP, Birmingham, 1989.
4. I.M. Robertson: *Mater. Forum*, 1991, vol. 15, pp. 102-11.
5. F. Barlat, S.M. Miyasato, J. Liu, and J.C. Brem: *Aluminium Alloys: Their Physical and Mechanical Properties*, (ICAA4) Conf. Proc., T.H. Sanders, Jr. and E.A. Starke, Jr., Georgia Institute of Technology, Atlanta, GA, 1994, p. 389.
6. P.J. Gregson and H.M. Flower: *Acta Metall.*, 1985, vol. 33, pp. 527-37.
7. N.E. Prasad and G. Malakondaiah: *Bull. Mater. Sci.*, 1992, vol. 15, pp. 297-310.
8. A.K. Vasudevan, M.A. Przystupa, and W.G. Fricke, Jr.: *Mater. Sci. Eng.*, 1995, vol. A196, pp. 1-8.
9. O. Engler, J. Mizera, J.H. Driver, and K. Lucke: *Textures Microstr.*, 1991, vols. 14–18, pp. 1153-58.
10. M.J. Bull and D.J. Lloyed: in *Aluminium Lithium Alloys III*, C. Baker, P.J. Gregson, S.J. Harris, and C.J. Peel, eds., The Institute of Metals, London, 1986, pp. 402-10.
11. A.A. Gokhale, V. Singh, D.V.A. Rao, and C.R. Chakravorty: DMRL Technical Report No. TR90111, Defence Metallurgical Research Laboratory, Hyderabad 1990.
12. A.W. Bowen: *Proc. 8th Int. Conf. on Textures of Materials*, J.S. Kallend and G. Gottsein, eds., TMS, Warrendale, PA, 1988, p. 971.
13. L.G. Schulz: *J. Appl. Phys.*, 1949, vol. 20, p. 1039.
14. H.J. Bunge: *Texture Analysis in Materials Science*, Butterworth and Co., London, 1982.
15. A.A. Gokhale, V. Singh, C.R. Chakravorty, K.S. Prasad, and D. Banerjee: *Met. Mater. Process*, 1990, vol. 2, pp. 267-78.
16. K. Lucke: *Proc. 6th Int. Conf. on Texture of Materials*, S. Nagashima, ed., Iron and Steel Institute of Japan, Tokyo, 1981, vol. 1, p. 14.
17. A.K. Vasudevan, W.G. Fricke, Jr., M.A. Przystupa, and S. Panchanadeeswaran: *Proc. 8th Int. Conf. on Textures of Materials*, J.S. Kallend and G. Gottstein, eds., TMS, Warrendale, PA, 1988, p. 1071.